

Dark radiation and dark matter coupled to holographic Ricci dark energy

Luis P. Chimento^a, Martín G. Richarte^b

Departamento de Física, Facultad de Ciencias Exactas y Naturales, Universidad de Buenos Aires and IFIBA, CONICET, Ciudad Universitaria, Pabellón I, 1428, Buenos Aires, Argentina

Received: 20 February 2013 / Published online: 9 April 2013
© Springer-Verlag Berlin Heidelberg and Società Italiana di Fisica 2013

Abstract We investigate a universe filled with interacting dark matter, holographic dark energy, and dark radiation for the spatially flat Friedmann–Robertson–Walker (FRW) spacetime. We use a linear interaction to reconstruct all the component energy densities in terms of the scale factor by directly solving the balance's equations along with the source equation. We apply the χ^2 method to the observational Hubble data for constraining the cosmic parameters, contrast with the Union 2 sample of supernovae, and analyze the amount of dark energy in the radiation era. It turns out that our model exhibits an excess of dark energy in the recombination era whereas the stringent bound $\Omega_x(z \simeq 10^{10}) < 0.21$ at big-bang nucleosynthesis is fulfilled. We find that the interaction provides a physical mechanism for alleviating the triple cosmic coincidence and this leads to $\Omega_{m0}/\Omega_{x0} \simeq \Omega_{r0}/\Omega_{x0} \simeq \mathcal{O}(1)$.

1 Introduction

The two main components of the universe are dark matter and dark energy. The dark matter accounts for 1/3 of the stuff in the universe and is also inextricably connected with the formation of galaxies and galaxy clusters. In fact this new form of matter not only holds galaxies together, but also is responsible for the large-structure formation in the universe [1, 2]. The astrophysical evidence for dark matter come from colliding galaxies, gravitational lensing of mass distribution or power spectrum of clustered matter [3–5].

The other 2/3 exists as in an even more mysterious form dubbed as dark energy and is causing the expansion of the Universe to speed up, rather than slow down. The first serious observational hints of dark energy in the universe date

back to the 1990s when astronomers observations of supernova were used to trace the expansion history of the universe [6–8]. Subsequently, the WMAP results suggested that the aforesaid amount of dark energy could explain both the flatness of the universe along with the observed accelerated expansion [9, 10]. Nowadays, there is a growing number of observational methods for probing the dynamical behavior of dark energy at different scales; galaxy redshift surveys allow to obtain the Hubble expansion history by measurement of baryon acoustic oscillation in the galaxy distribution [1, 2], geometric weak lensing method applied to Hubble space telescope images helps to find tighter constraints on the dark energy equation of state also [11].

Despite the devoted effort for understanding the nature of dark matter and dark energy, there was not found a microscopic theory for the dark side of the universe, capable of unraveling their particles content. On the observational side, the data of several tests have confirmed some of their plausible properties, such as that it could be the repulsive effect of dark energy or the clustering action of dark matter.

Another interesting trait to explore is related with the existence of non-gravitational coupling between dark matter and dark energy, such exchange of energy could alter the cosmic history, leaving testable imprints in the universe [12]. It is believed that a coupling between dark energy and dark matter changes the background evolution of the dark sector allowing to constrain any type of interaction and giving rise to a richer cosmological dynamics compared with non-interacting models [12]. A step forward for constraining dark matter and dark energy is to use the physics behind recombination or big-bang nucleosynthesis epochs by adding a decoupled radiation term to the dark sector for taking into account the stringent bounds related to the behavior of dark energy at early times [13, 14]. The behavior of dark energy in the recombination era was explored within the framework of three interacting components also [15].

^a e-mail: chimento@df.uba.ar

^b e-mail: martin@df.uba.ar

Our goal is to consider a model where dark matter and dark radiation are coupled to holographic dark energy and explore the cosmic triple coincidence problem related to the amount of these components at present [16]. We perform a cosmological constraint using the updated Hubble data [17], numerically obtain the distance modulus $\mu(z)$ for contrasting with the Union 2 compilation of supernovae Ia [18], and analyze the order of magnitude corresponding to the cosmological parameter known as transition redshift. In order to check the feasibility of the model, we also examine the severe bounds for dark energy in the recombination era [19] or nucleosynthesis epoch [20].

2 The model

We consider a spatially flat homogeneous and isotropic universe described by FRW spacetime with line element given by $ds^2 = -dt^2 + a^2(t)(dx^2 + dy^2 + dz^2)$ being $a(t)$ the scale factor. The universe is filled with three interacting fluids namely, dark radiation, dark matter and modified holographic Ricci dark energy so that the evolution of the FRW universe is governed by the Friedmann and conservation equations, respectively,

$$3H^2 = \rho_r + \rho_m + \rho_x, \quad (1)$$

$$\dot{\rho} + 3H(\rho_r + p_r + \rho_m + p_m + \rho_x + p_x) = 0, \quad (2)$$

where a is the scale factor and $H = \dot{a}/a$ stands for the Hubble expansion rate. Here, we will use the holographic principle within the cosmological context by associating the infrared cutoff L with the dark energy density, thus we take L^{-2} in the form of a linear combination of \dot{H} and H^2 :

$$\rho_x = \frac{2}{\alpha - \beta} \left(\dot{H} + \frac{3\alpha}{2} H^2 \right). \quad (3)$$

Here, α and β are two free constants. In particular, we obtain $\rho_x \propto R$ for $\alpha = 4/3$, where $R = 6(\dot{H} + 2H^2)$ is the Ricci scalar curvature for a spatially flat FRW space-time.

The use of the variable $\eta = \ln(a/a_0)^3$, where a_0 is set as the value of the scale factor at present and $' \equiv d/d\eta$, allows us to rewrite Eqs. (2) and (3) as

$$\rho' = -\gamma_r \rho_r - \gamma_m \rho_m - \gamma_x \rho_x, \quad (4)$$

$$\rho' = -\alpha \rho_c - \beta \rho_x, \quad (5)$$

$$\rho_c = \rho_r + \rho_m, \quad (6)$$

where $\gamma_i = 1 + p_i/\rho_i$ denotes the barotropic index, not necessarily constant, of each component with $i = \{r, m, x\}$, $\gamma_r \simeq 4/3$, $\gamma_m \simeq 1$, $0 < \gamma_x < 2/3$ so that $0 < \gamma_x < \gamma_m < \gamma_r$. Taking into account Eq. (5) along with Eq. (6), we could extract as a physical hint that the modified holographic dark energy (3) forces to the dark matter and dark radiation to have the same bare equation of state.

The holographic dark energy (3) or (5) looks like a ‘‘conservation equation’’ for the three dark components with constant coefficients. Therefore, the selected holographic dark energy (3) or (5) has transformed the original model of three interacting components into another simpler scheme of two interacting components having two constant equations of state. As we have already mentioned above, such degeneration occurs because the dark radiation and dark matter have the same equation of state, $p_r = (\alpha - 1)\rho_r$ and $p_m = (\alpha - 1)\rho_m$. After comparing the whole conservation equation (4) with modified conservation equation (5), we obtain the compatibility relation

$$\gamma_r \rho_r + \gamma_m \rho_m + \gamma_x \rho_x = \alpha(\rho_r + \rho_m) + \beta \rho_x, \quad (7)$$

that relates the equation of state of the dark components with the bare ones. In what follows, we will use Eq. (5) with constant coefficients α and β instead of Eq. (4) with the non-constant coefficient $\gamma_x = 1 + p_x/\rho_x$. In some sense, (4) and (5) give rise to different representations of the mixture of two interacting fluids and clearly these descriptions are related between them by the compatibility relation (7). Therefore, the holographic dark energy (3) conveniently links a model of three interacting fluids having *variable equations of state* with a model of two interacting fluids with ‘‘bare constant equations of state’’.

Solving the system of equations $\rho = \rho_c + \rho_x$ and (5) we get the energy densities of both component as a function of ρ and its derivative ρ'

$$\rho_c = -\frac{\beta\rho + \rho'}{\Delta}, \quad \rho_x = \frac{\alpha\rho + \rho'}{\Delta}, \quad (8)$$

where $\Delta = \alpha - \beta$ is the determinant of the linear equation system and we assume that $\beta < \alpha$. Now, we introduce energy transfer between those components by splitting Eq. (5) into two balance equations

$$\rho'_c + \alpha\rho_c = -Q, \quad (9)$$

$$\rho'_x + \beta\rho_x = Q, \quad (10)$$

where we have considered a coupling with a factorized H dependence $3HQ$, being Q the interaction term that generates the energy transfer between the two fluids. After differentiating the first Eq. (8) and combining with Eq. (9), we obtain a second order differential equation for the total energy density (source equation)

$$\rho'' + (\alpha + \beta)\rho' + \alpha\beta\rho = Q\Delta. \quad (11)$$

We will take into account interactions Q for which the solutions of the evolution equation for the scale factor $H = \sqrt{\rho/3}$ includes power law ones, because they play an essential role for determining the asymptotic behavior of the effective barotropic index $\gamma = (\alpha\rho_c + \beta\rho_x)/\rho = -2\dot{H}/3H^2$. It describes a universe approaching to a stationary stage γ_s associated with the constant solution $\gamma = \gamma_s$, where $0 < \beta <$

$\gamma_s < \alpha$ and $a = t^{2/3\gamma_s}$. In addition, given a set of initial conditions, if γ tends asymptotically to the constant solution γ_s , then γ_s becomes an attractor solution [12]. An interaction satisfying this requirement belongs to the class

$$Q = \frac{(\gamma_s - \alpha)(\gamma_s - \beta)}{\Delta} \rho, \tag{12}$$

with $Q < 0$ [12]. Solving the source equation (11) for this interaction, we obtain the total energy density

$$\rho = ca^{-3\gamma_s} + ba^{-3(\alpha+\beta-\gamma_s)}. \tag{13}$$

Hence, for any initial conditions c, b , and large scale factor, the energy density behaves as $c/a^{3\gamma_s}$ and the power-law expansion $a \rightarrow t^{2/3\gamma_s}$ becomes asymptotically stable.

The dark densities of coupled components, ρ_x and ρ_c , are given by

$$\rho_c = \frac{(\gamma_s - \beta)ca^{-3\gamma_s} + (\alpha - \gamma_s)ba^{-3(\alpha+\beta-\gamma_s)}}{\Delta}, \tag{14}$$

$$\rho_x = \frac{(\alpha - \gamma_s)ca^{-3\gamma_s} + (\gamma_s - \beta)ba^{-3(\alpha+\beta-\gamma_s)}}{\Delta}. \tag{15}$$

Thus, the ratio $r = \rho_c/\rho_x$ tends to $r_s = (\gamma_s - \beta)/(\alpha - \gamma_s)$, being r_s an attractor.

With the aid of the total energy density (13), we can calculate the explicit form of the interaction term (12) as a function of the scale factor,

$$Q = \frac{(\gamma_s - \alpha)(\gamma_s - \beta)}{\Delta} [ca^{-3\gamma_s} + ba^{-3(\alpha+\beta-\gamma_s)}]. \tag{16}$$

In turn Eq. (9) can be rewritten as

$$\rho'_r + \rho'_m + \alpha(\rho_r + \rho_m) = -Q. \tag{17}$$

In order to break the degeneracy of this set of components, formed by dark radiation and dark matter, we introduce partial interactions into the corresponding balance equation of both components as follows:

$$\rho'_r + \alpha\rho_r = Q_r, \tag{18}$$

$$\rho'_m + \alpha\rho_m = Q_m, \tag{19}$$

where Q_r and Q_m stand for the exchange of energy between ρ_r and ρ_x , and besides these satisfy the condition

$$Q + Q_m + Q_r = 0, \tag{20}$$

to recover the conservation equation (5) after having summed all Eqs. (17)–(19). Also we assume that Q_r and Q_m are a linear combination of the two terms contained in the interaction term Q (16), so they read

$$Q_r = c_1a^{-3\gamma_s} + b_1a^{-3(\alpha+\beta-\gamma_s)}, \tag{21}$$

$$Q_m = -(c_1 + Q_0c)a^{-3\gamma_s} - (b_1 + Q_0b)a^{-3(\alpha+\beta-\gamma_s)}, \tag{22}$$

where $Q_0 = (\gamma_s - \alpha)(\gamma_s - \beta)/\Delta$, while c_1 and b_1 are free parameters of the model. Inserting these interactions into the evolution equation of the dark radiation and dark matter (18)–(19) and solving these coupled system of equations we obtain

$$\rho_r = \frac{c_1a^{-3\gamma_s}}{\alpha - \gamma_s} - c_0a^{-3\alpha} + \frac{b_1a^{-3(\alpha+\beta-\gamma_s)}}{\gamma_s - \beta}, \tag{23}$$

$$\rho_m = -\frac{(c_1 + Q_0c)a^{-3\gamma_s}}{\alpha - \gamma_s} + c_0a^{-3\alpha} - \frac{(b_1 + Q_0b)a^{-3(\alpha+\beta-\gamma_s)}}{\gamma_s - \beta}, \tag{24}$$

where the first and third terms in both dark energies densities are the particular solutions of the evolution equations (18) and (19) while the second term, in both Eqs. (23) and (24) is the homogeneous solution of the linear system of Eqs. (18) and (19). In what follows, we fix $c_1 = -Q_0c/2 > 0$ and $b_1 = -Q_0b/2 > 0$ without loss of generality. Using Eqs. (14), (15), (23), and (24), we find the coefficients c, b , and c_0 in terms of the density parameters and γ_s . Now, we only show their expressions for $\alpha = 4/3$ and $\alpha + \beta - \gamma_s = 1$:

$$c = 3H_0^2 \left[\frac{1 + \Omega_{x0}(3\gamma_s - 5)}{3(\gamma_s - 1)} \right], \tag{25}$$

$$b = 3H_0^2 \left[\frac{(5\Omega_{x0} - 4) + 3\gamma_s(1 - \Omega_{x0})}{3(\gamma_s - 1)} \right], \tag{26}$$

$$c_0 = 3H_0^2 \left[\frac{1 - \Omega_{x0} - 2\Omega_{m0}}{2} \right]. \tag{27}$$

Here, Ω_{i0} stands for the density parameter of each component.

3 Observational constraints on the three interacting model

We will provide a qualitative estimation of the cosmological parameters by constraining them with the Hubble data [21–23] and the strict bounds for the behavior of dark energy at early times [19]. In the former case, the statistical analysis is based on the χ^2 -function of the Hubble data which is constructed as (e.g. [24])

$$\chi^2(\theta) = \sum_{k=1}^{19} \frac{[H(\theta, z_k) - H_{\text{obs}}(z_k)]^2}{\sigma(z_k)^2}, \tag{28}$$

where θ stands for cosmological parameters, $H_{\text{obs}}(z_k)$ is the observational $H(z)$ data at the redshift z_k , $\sigma(z_k)$ is the corresponding 1σ uncertainty, and the summation is over the 19 observational $H(z)$ data [17]. Using the absolute ages of passively evolving galaxies observed at different redshifts, one obtains the differential ages dz/dt and the function $H(z)$ can be measured through the relation $H(z) = -(1+z)^{-1} dz/dt$ [21–23]. The data $H_{\text{obs}}(z_i)$ and $H_{\text{obs}}(z_k)$ are uncorrelated because they were obtained from the observations of galaxies at different redshifts.

From Eq. (13) one finds that the Hubble expansion of the model becomes

$$H(\theta|z) = H_0(Cx^{3\gamma_s} + Bx^{3(\alpha+\beta-\gamma_s)})^{\frac{1}{2}}, \tag{29}$$

where $c = 3H_0^2C$, $b = 3H_0^2B$ as obtained from (25), (26), respectively. Here, we consider $\theta = \{H_0, \gamma_s, \Omega_{x0}\}$ as the independent parameters to be constrained for the model encoded in the Hubble function (29) with the statistical estimator (28), while α is taken equal to $4/3$ to have an early era dominated by radiation. Besides, we will impose $\alpha + \beta - \gamma_s = 1$ so that the universe exhibits an intermediate stage dominated by pressureless dark matter. For a given pair of (θ_1, θ_2) , we are going to perform the statistic analysis by minimizing the χ^2 function to obtain the best fit values of the random variables $\theta_{\text{crit}} = \{\theta_{\text{crit}1}, \theta_{\text{crit}2}\}$, which correspond to a minimum of Eq. (28). Then, the best-fit parameters θ_{crit} are those values where $\chi_{\text{min}}^2(\theta_{\text{crit}})$ leads to the local minimum of the $\chi^2(\theta)$ distribution. If $\chi_{\text{d.o.f}}^2 = \chi_{\text{min}}^2(\theta_{\text{crit}})/(N - n) \leq 1$ the fit is good and the data are consistent with the considered model $H(z; \theta)$. Here, N is the number of data and n is the number of parameters [24]. The variable χ^2 is a random variable that depends on N and its probability distribution is a χ^2 distribution for $N - n$ degrees of freedom. Here $N = 19$ and $n = 3$, so in principle, we will perform three minimizations of the χ^2 statistical estimator, interpreting the goodness of fit by checking the condition $\chi_{\text{d.o.f}}^2 < 1$; as a way to keep the things clear and focus on extracting relevant physical information from this statistical estimation.

The random datasets that satisfy the inequality $\Delta\chi^2 = \chi^2(\theta) - \chi_{\text{min}}^2(\theta_{\text{crit}}) \leq 2.30$ also represent 68.3 % confidence contours in the 2D plane at 1σ level. It can be shown that 95.4 % confidence contours with a 2σ error bar in the

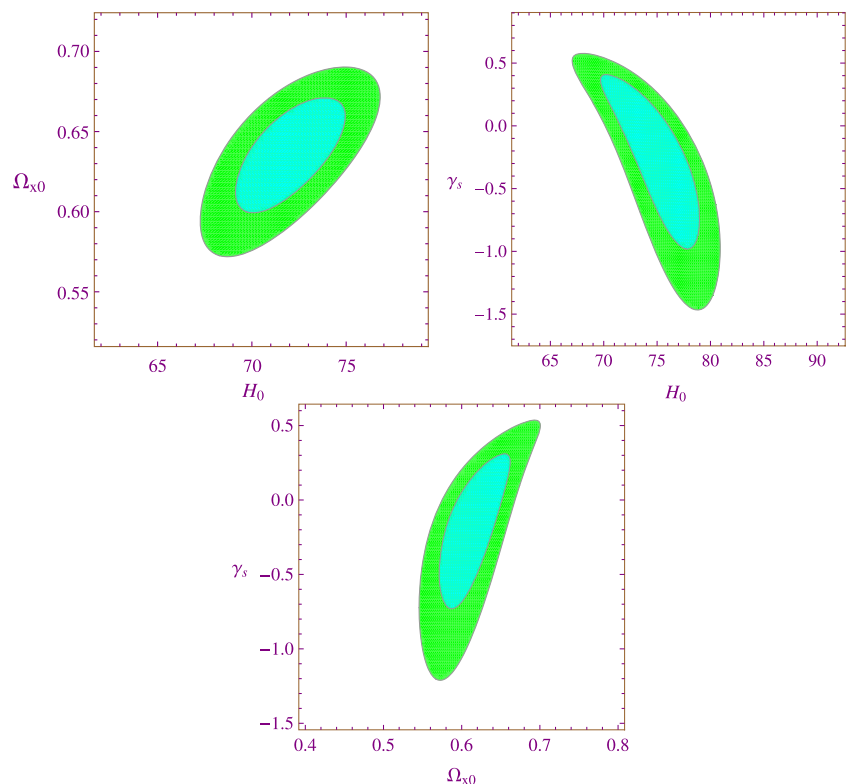
samples satisfy $\Delta\chi^2 \leq 6.17$. The two-dimensional C.L. obtained with the standard χ^2 function for two independent parameters is shown in Fig. 1, whereas the estimation of these cosmic parameters is briefly summarized in Table 1.

We obtain $\gamma_s \leq 10^{-3}$, so these values clearly fulfill the constraint $\gamma_s < 2/3$, which ensures the existence of an accelerated phase of the universe at late times [Table 1]. We find the best fit at $(H_0, \Omega_{x0}) = (72.05^{+2.90}_{-2.93} \text{ km s}^{-1} \text{ Mpc}^{-1}, 0.637^{+0.033}_{-0.038})$ with $\chi_{\text{d.o.f}}^2 = 0.81$ by using the prior $\gamma_s = 10^{-3}$. These findings show, in broad terms, that the estimated values of H_0 and Ω_{x0} are in agreement with the standard ones reported by the WMAP-7 project [26]. The value of Ω_{x0} is slightly lower than the standard one of 0.7 being such discrepancy less or equal to 0.1 %. We find that using the priors $H_0 = 70.4 \text{ km s}^{-1} \text{ Mpc}^{-1}$ the best-fit values for the present-day density parameters are $(\Omega_{x0}, \Omega_{r0}) = (0.62, 7 \times 10^{-2})$ along with a larger goodness condition

Table 1 Observational bounds for the 2D C.L. obtained in Fig. 1 by varying two cosmological parameters. The $\chi_{\text{d.o.f}}^2$ in all the cases studied is less the unity; in fact it goes from 0.81 to 0.94

2D Confidence level		
Priors	Best fits	$\chi_{\text{d.o.f}}^2$
$\gamma_s = 10^{-3}$	$(H_0, \Omega_{x0}) = (72.05^{+2.90}_{-2.93}, 0.637^{+0.033}_{-0.038})$	0.81
$\Omega_{x0} = 0.67$	$(H_0, \gamma_s) = (73.81^{+5.14}_{-4.24}, 0.001^{+0.404}_{-0.984})$	0.94
$H_0 = 70.4$	$(\Omega_{x0}, \gamma_s) = (0.623^{+0.038}_{-0.051}, 0.001^{+0.310}_{-0.732})$	0.86

Fig. 1 Two-dimensional C.L. associated with $1\sigma, 2\sigma$ for different θ planes



($\chi^2_{d.o.f} = 0.86$) [Table 1]. Regarding the amount of dark matter at present, we have fixed $\Omega_{m0} = 0.3$ because this value is consistent with one reported by the WMAP-7 project [26]. In performing the statistical analysis, we find that $H_0 \in [70.4, 73.81] \text{ km s}^{-1} \text{ Mpc}^{-1}$ so the estimated values are met within 1σ C.L. reported by Riess et al. [25], to wit, $H_0 = (72.2 \pm 3.6) \text{ km s}^{-1} \text{ Mpc}^{-1}$. In order to ensure that our previous local minimization analysis is correct, we have performed a global statistical analysis by estimating all the parameters at once. In doing that, we obtain $(H_0, \Omega_{x0}, \gamma_s) = (72.05, 0.63, 10^{-3})$ along with $\chi^2_{d.o.f} = 0.86 < 1$ [see Fig. 2]. Figure 2 shows two-dimensional C.L. in the $\Omega_{x0}-\gamma_s$ plane obtained when the joint probability $P(H_0, \Omega_{x0}, \gamma_s)$ is marginalized over H_0 (see Fig. 2); then the marginalized best-fit values become $(\Omega_{x0}, \gamma_s) = (0.619^{+0.052}_{-0.023}, 0.001^{+0.239}_{-0.239})$ with $\chi^2_{d.o.f} = 0.87 < 1$. It must be stressed that we report for the most relevant minimization procedures the corresponding marginal 1σ error bars [27], as can be seen in Table 1.

As is well known, distance indicators can be used for confronting distance measurements to the corresponding model predictions. Among the most useful ones are those objects of known intrinsic luminosity such as standard candles, so that the corresponding comoving distance can be determined. That way, it is possible to reconstruct the Hubble expansion rate by searching this sort of object at different redshifts. The most important class of such indicators is type Ia supernovae. Then, we would like to compare the Hubble data with the Union 2 compilation of 557 SNe Ia [18] by contrasting theoretical distance modulus with the observational dataset. In order to do that, we note that the apparent magnitude of a supernova placed at a given redshift z is related to the expansion history of the Universe through the distance modulus

$$\mu \equiv m - M = 5 \log \frac{d_L(z)}{h} + \mu_0, \tag{30}$$

where m and M are the apparent and absolute magnitudes, respectively, $\mu_0 = 42.38$, $h = H_0/100 \text{ km}^{-1} \text{ s}^{-1}$, and

$d_L(z) = H_0(1+z)r(z)$, $r(z)$ being the comoving distance, given for a FRW metric by

$$r(z) = \int_0^z \frac{dz'}{H(z')}. \tag{31}$$

Using the Union 2 dataset, we will obtain five Hubble diagrams and compare each of them with the theoretical distance modulus curves that represent the best-fit cosmological models found with the update Hubble data (see Fig. 3); it turned out that at low redshift ($z < 1.4$) there is an excellent agreement between the theoretical model and the observational data.

For the sake of completeness, we also report bounds for other cosmological relevant parameters [see Table 2], such as the fraction of dark radiation $\Omega_r(z=0)$, the effective equation of state at $z=0$ ($\omega_{\text{eff}0} = \gamma_{\text{eff}0} - 1$), decelerating parameter at the present time q_0 , and the transition redshift (z_c) among many others, all these quantities are derived using the three best fit values reported in Table 1. We find that the z_c is of the order unity varying over the interval $[0.68, 0.93]$, such values are close to $z_c = 0.69^{+0.20}_{-0.13}$ reported in [28–32] quite recently. Moreover, taking into account a χ^2 -statistical analysis made in the (ω_0, z_c) -plane based on the supernova sample (Union 2) it has been shown that at 2σ C.L. the transition redshift varies from 0.60 to 1.18 [33]. In order to estimate z_c as independent parameter using a χ^2 method, we first needed to obtain its generic formula by imposing the condition $(z_c + 1)H'(z_c) = H(z_c)$:

$$z_c = \left(\frac{3\Omega_{x0}(1-\gamma_s) + (4-3\gamma_s)}{(2-3\gamma_s)[3\Omega_{x0}(1-\gamma_s) + 1]} \right)^{1/3(1-\gamma_s)} - 1. \tag{32}$$

Hence, placing Eq. (32) into Eq. (29), the Hubble parameter turns out to be a function of H_0, z_c , and γ_s . The global statistical analysis using z_c as independent parameter instead of Ω_{x0} leads to $(H_0, z_c, \gamma_s) = (72.05, 0.63, 10^{-3})$ along with $\chi^2_{d.o.f} = 0.86$ [see Fig. 4] whereas the marginalized best-fit values become $(z_c, \gamma_s) = (0.623^{+0.039}_{-0.052}, 0.001^{+0.313}_{-0.733})$ with a $\chi^2_{d.o.f} = 0.86$ [see Fig. 4]; notice that the marginalized best fit value of z_c is considerably lower than the values reported in Table 2. Besides, the behavior of decelerating parameter

Fig. 2 (Left panel): Three-dimensional C.L. for the $H_0-\gamma_s-\Omega_{x0}$ plane. (Right panel): Two-dimensional C.L. obtained after have performed the marginalization over H_0

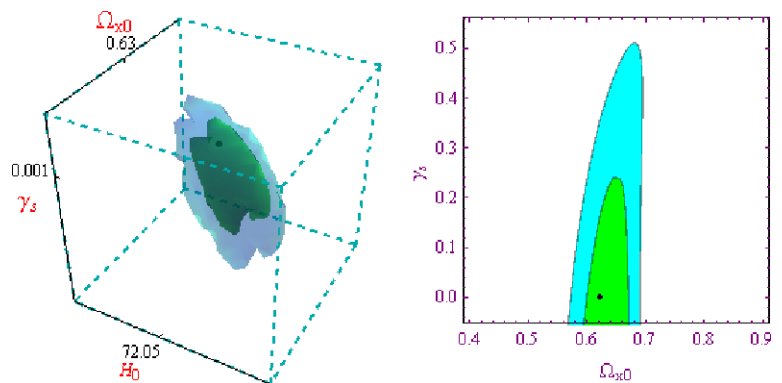


Fig. 3 Hubble diagram for the Union 2 compilation: the *points* are the observational data of supernovae, the theoretical curves $\mu(z)$ (*dashed lines*) represent the best cosmological model for different cases:

(global estimation):

$$I (H_0, \Omega_{x0}, \gamma_s) = (72.05, 0.63, 0.001),$$

(marginalizing over H_0)

$$II (\Omega_{x0}, \gamma_s) = (0.619^{+0.052}_{-0.023}, 0.001^{+0.239}_{-0.239}),$$

$$III (H_0, \Omega_{x0}) = (72.05^{+2.90}_{-2.93}, 0.637^{+0.033}_{-0.038}),$$

$$IV (H_0, \gamma_s) = (73.81^{+5.14}_{-4.24}, 0.001^{+0.404}_{-0.984}),$$

$$V (\Omega_{x0}, \gamma_s) = (0.623^{+0.038}_{-0.051}, 0.001^{+0.310}_{-0.732})$$

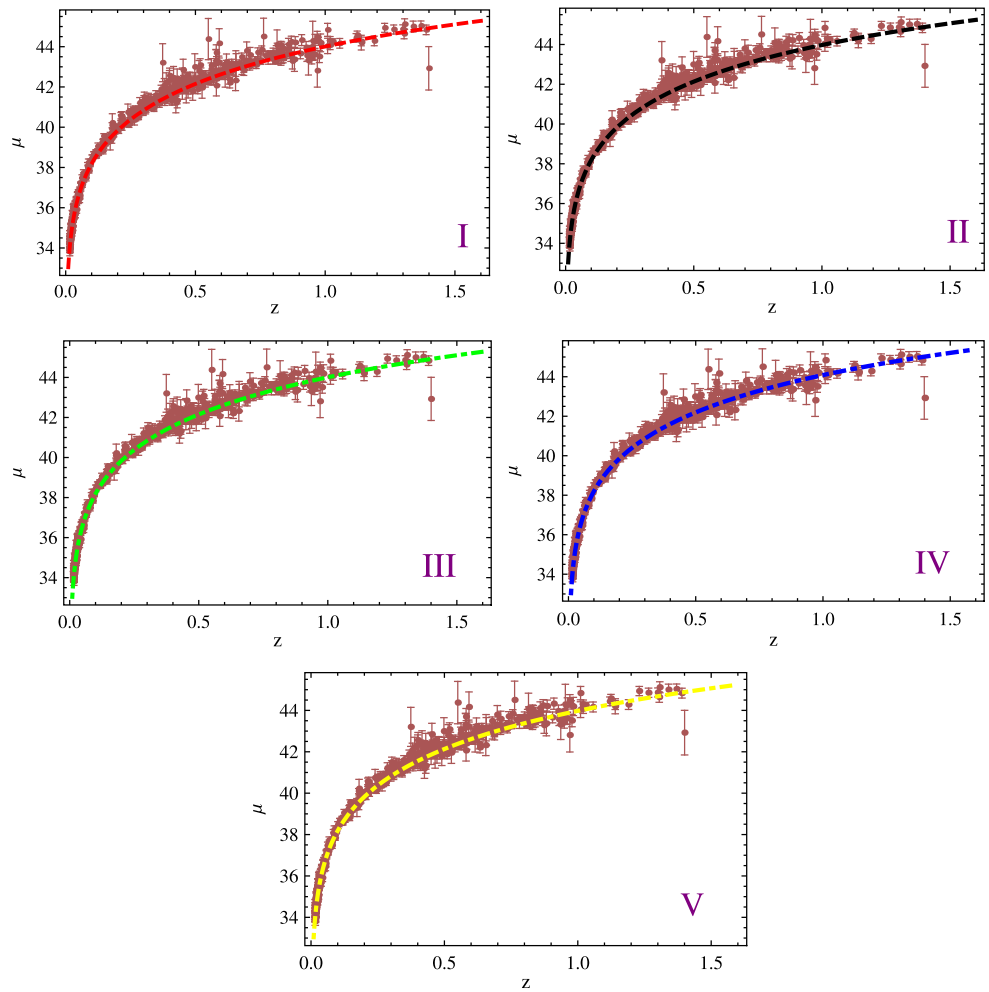


Fig. 4 (Upper panel): Three-dimensional C.L. for the H_0 - γ_s - z_c plane. (Lower panel): Two-dimensional C.L. obtained after have performed the marginalization over H_0

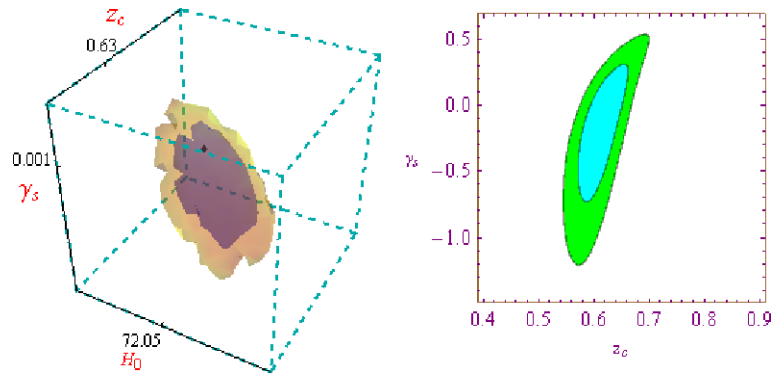


Table 2 Derived bounds for cosmic parameters using the best fits value of 2D C.L. obtained in Table 1 by varying two cosmological parameters in three different cases

Bounds for cosmological parameters										
θ_c	z_c	$q(z=0)$	$\omega_{\text{ove}}(z=0)$	$\omega_{\text{eff},x}(z=0)$	$\Omega_x(z \simeq 1100)$	$\Omega_x(z \simeq 10^{10})$	Ω_{m0}	Ω_{r0}	Ω_{m0}/Ω_{x0}	Ω_{r0}/Ω_{x0}
I	0.75	-0.59	-0.64	-1.32	0.26	0.26	0.3	0.062	0.47	0.09
II	0.93	-0.67	-0.74	-1.23	0.23	0.23	0.3	0.03	0.44	0.04
III	0.68	-0.55	-0.70	-1.28	0.20	0.20	0.3	0.07	0.48	0.1

with redshift is shown in Fig. 4, in particular, its present-day value varies as $-0.67 < q_0 < -0.55$ for the three cases mentioned in Table 2, and all these values are in perfect agreement with the one reported by WMAP-7 project [26].

The effective EOS of the mix is given by

$$\omega_{\text{eff}} = \frac{\beta\Omega_x + \alpha\Omega_m + \alpha\Omega_r}{\sum_i \Omega_i} - 1. \tag{33}$$

The effective equation of state (EOS) for dark energy is obtained from Eq. (10), it reads

$$\omega_{\text{eff}x} = \left(\gamma_x - \frac{Q_x}{\rho_x} \right) - 1. \tag{34}$$

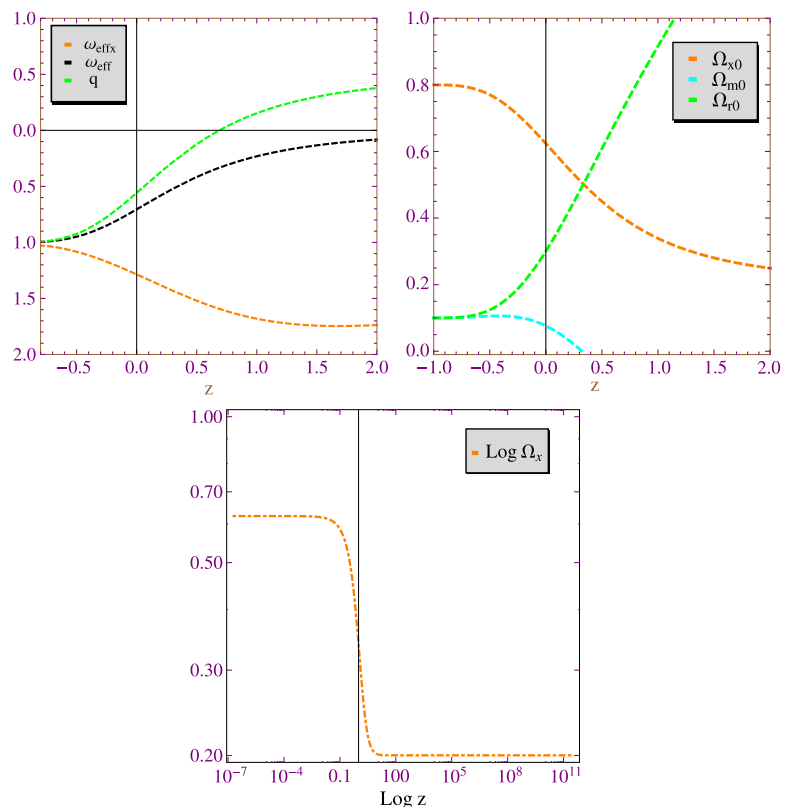
In Fig. 5 we plot the effective equation of state as a function of redshift for the best-fit value shown in Table 1, in general, we find that $\omega_{\text{eff}} \geq -1$ provided that $(1 - 3\gamma_s)\Omega_x + 4(\Omega_r + \Omega_m) \leq 3$, as a matter of fact its present-day values cover the range $[-0.74, -0.64]$. On the other hand, the effective EOS associated to the dark energy evaluated at $z = 0$, $\omega_{\text{eff}x}(z = 0)$ varies over the range $[-1.32, -1.23]$.

In regard to the behavior of density parameters Ω_x , Ω_m , and Ω_r , we see that very close to $z = 0$ the dark energy is the main agent that speeds up the universe, far away from $z = 1$ the universe is dominated by the dark matter and at very early times the radiation component governs the entire dynamic of the universe around $z \simeq 10^3$ [cf. Fig. 5]. In this point, we would like to present an appealing discussion concerning the triple cosmic coincidence problem (TCC) [16]

related to the amount of dark energy, dark matter, and radiation at present moment. We have proposed a physical mechanism based on a phenomenological interaction among the three cosmic components, in fact, since we are working within the framework of three interacting cosmic components the aforesaid scenario seems to be a fertile arena for studying the TCC. As pointed out by Arkani-Hamed et al. in their seminal work: “there is an era in the history of the universe where all three forms of energy, in matter, radiation and dark energy, become comparable within a few orders of magnitude” [16]. Here, we have found that interaction made it possible to have $\Omega_{m0}/\Omega_{x0} = 0.3/0.62 = 0.48$ and $\Omega_{r0}/\Omega_{x0} = 0.07/0.62 = 0.11$, so $\Omega_{m0}/\Omega_{x0} \simeq \Omega_{r0}/\Omega_{x0} \simeq \mathcal{O}(1)$, showing that the interaction implemented can be used for alleviating the TCC [see Table 2].

Now, we explore another kind of constraint, which comes from the physics at early times because this can be considered as a complementary tool for testing our model. As is well known the fraction of dark energy in the recombination epoch should fulfill the bound $\Omega_{\text{ede}}(z \simeq 1100) < 0.1$. Taking into account the best-fit values reported in Table 1, we find that at early times the dark energy does not change much with the redshift z over the interval $[10^3, 10^{10}]$, in fact, the $\text{Log } \Omega_x$ in terms of $\text{Log } z$ goes from 0.64 to 0.20 [see Fig. 5]. Table 2 shows that around $z \simeq 1100$ (recombination) Ω_x can vary from 0.20 to 0.26. This excess of dark energy requires further research because some signal

Fig. 5 Plots of $\Omega_x(z)$, $\Omega_m(z)$, $\Omega_r(z)$, $q(z)$, $\omega_{\text{eff}}(z)$, $\omega_{\text{eff}x}(z)$ using the best-fit values obtained with the Hubble data for different θ planes. Plot of $\text{Log } \Omega_x$ in terms of $\text{Log } z$



could arise from this early dark energy (EDE) models uncovering the nature of DE as well as their properties to high redshift, giving an invaluable guide to the physics behind the recent speed up of the universe [14, 19]. Regarding the values reached by Ω_x around the big bang nucleosynthesis (BBN) $z = 10^{10}$, we find that there is a variation from 0.20 to 0.26, so the conventional BBN processes that occurred at temperature of 1 Mev is not spoiled because the severe bound reported for early dark energy $\Omega_x(z \simeq 10^{10}) < 0.21$ is marginally fulfilled at BBN [20].

As is well known, dark energy dominates the whole dynamics of the universe at present and there is an obvious decoupling with radiation practically. However, from a theoretical point of view, it is reasonable to expect that dark components can interact with other fluids of the universe substantially in the very beginning of its evolution due to processes occurring in the early universe. For instance, dark energy interacting with neutrinos was investigated in [34]. The framework of many interacting components could provide a more natural arena for studying the stringent bounds of dark energy at recombination epoch. There could be a signal in favor of having dark matter exchanging energy with dark energy while radiation is treated as a decoupled component [13, 14] or the case where dark matter, dark energy, and radiation exchange energy. More precisely, when the universe is filled with interacting dark sector plus a decoupled radiation term, it was found that $\Omega_x(z \simeq 1100) = 0.01$ [13] or $\Omega_x(z \simeq 1100) = 10^{-8}$ [14] but if radiation is coupled to the dark sector, the amount of dark energy is drastically reduced, giving $\Omega_x(z \simeq 1100) \simeq \mathcal{O}(10^{-11})$ [15]. In our model, we have found that the amount of early dark energy varies in the range [0.26; 0.20], so the behavior of dark energy at recombination is considerably much smoother than in the aforesaid cases [13–15]. We expect to include a (decoupled) neutrino term in the Friedmann equation to examine in more detail the dark radiation as a signature of dark energy.

4 Conclusion

We have discussed a class of interacting dark matter, dark radiation, and holographic Ricci-like dark energy model for a spatially flat FRW background. We have coupled those components and obtained their energy densities in terms of the scale factor.

We have examined the previous model by constraining the cosmological parameters with the Hubble data and the well-known bounds for dark energy at recombination era. In the case of two-dimensional (2D) C.L., we have made three statistical constraints with the Hubble function [see Fig. 1 and Table 1]. We have found that $\gamma_s \leq 10^{-3}$, so these values fulfill the constraint $\gamma_s < 2/3$ for getting an accelerated phase of the universe at late times. We find the best fit at

$(H_0, \Omega_{x0}) = (72.05_{-2.93}^{+2.90} \text{ km s}^{-1} \text{ Mpc}^{-1}, 0.637_{-0.038}^{+0.033})$ with $\chi_{\text{d.o.f}}^2 = 0.81$ by using the prior $\gamma_s = 10^{-3}$. It turned out that the estimated values of H_0 and Ω_{x0} are in agreement with the standard ones reported by the WMAP-7 project [26]. Besides, we have found that $H_0 \in [70.4, 73.81] \text{ km s}^{-1} \text{ Mpc}^{-1}$, so the estimated values are met within 1σ C.L. reported by Riess et al. [25], to wit, $H_0 = (72.2 \pm 3.6) \text{ km s}^{-1} \text{ Mpc}^{-1}$. After having marginalized the joint probability $P(H_0, \Omega_{x0}, \gamma_s)$ over H_0 [see Fig. 1], we saw that the marginalized best-fit values are $(\Omega_{x0}, \gamma_s) = (0.619_{-0.023}^{+0.052}, 0.001_{-0.239}^{+0.239})$ with a $\chi_{\text{d.o.f}}^2 = 0.87 < 1$ [see Fig. 2]. Using the best fits mentioned in Table 1, we have numerically obtained the distance modulus of the supernova as predicted by the theoretical model and compare with the Union 2 dataset, finding that at low redshift ($z < 1.4$) there is excellent agreement between the theoretical model and the observational data [see Fig. 3].

Regarding the derived cosmological parameters, for instance, the transition redshift z_c turned out to be of the order unity varying over the interval [0.68, 0.93], such values are in agreement with $z_c = 0.69_{-0.13}^{+0.20}$ reported in [28–32], and meets within the 2σ C.L. obtained with the supernovae (Union 2) data in [33]. We also have performed a global statistical analysis using z_c as independent parameter instead of Ω_{x0} , which lead to $(H_0, z_c, \gamma_s) = (72.05, 0.63, 10^{-3})$ along with $\chi_{\text{d.o.f}}^2 = 0.86$ [see Fig. 4], whereas the marginalized best-fit values are $(z_c, \gamma_s) = (0.623_{-0.052}^{+0.039}, 0.001_{-0.733}^{+0.313})$ together with a $\chi_{\text{d.o.f}}^2 = 0.86$ [see Fig. 4]. Besides, with the decelerating parameters $q(z=0) \in [-0.67, -0.55]$ for the three cases mentioned in Table 2, all these values are perfectly in agreement with the one reported by WMAP-7 project [26] [see Fig. 5].

Concerning the effective equation of state, we have found that $\omega_{\text{eff}} > -1$ and its present-day values vary over the ranges $[-0.74, -0.64]$ [see Table 2 and Fig. 5]. The equation of state associated with dark energy satisfies the inequality $\omega_{\text{eff}x} \leq -1$.

Besides, we have found that the fraction of dark radiation at present moment, Ω_{r0} , varies in the interval [0.03, 0.07] for the three cases mentioned in Table 2. The dark energy amount $\Omega_x(z)$ governs the dynamic of the universe near $z = 0$, whereas far away from $z = 1$ the universe is dominated by the fraction of dark matter $\Omega_m(z)$ and at very early times the fraction of radiation $\Omega_r(z)$ controls the entire dynamic of the universe around $z \simeq 10^3$ [cf. Fig. 5]. We also have examined the triple cosmic coincidence problem [16] within the framework of three interacting cosmic components, finding that interaction used in this work provides a phenomenological mechanism for alleviating TCC, leading to $\Omega_{m0}/\Omega_{x0} \simeq \Omega_{r0}/\Omega_{x0} \simeq \mathcal{O}(1)$ [see Table 2].

Finally, we have found that at early times the dark energy does not change much with the redshift z over the interval $[10^3, 10^{10}]$, in fact, the $\text{Log } \Omega_x$ in terms of $\text{Log } z$ goes from 0.64 to 0.20 [see Fig. 5]. Table 2 shows that around $z \simeq 1100$

(recombination) Ω_x can vary from 0.20 to 0.26. The latter results indicate an excess of dark energy so it requires further research [14, 19], in fact it could be related with the degeneracy presents in the equation of states of dark matter and dark radiation. In order to explore this issue in more detail, we expect to include an additional (decoupled) neutrino term in Friedmann equation; thereby, we will seek to distinguish the radiation term coupled to dark matter, where both component share the same bare equation of state, from the decoupled neutrino term. However, it must be stressed that the values reached by Ω_x around the big-bang nucleosynthesis (BBN) $z = 10^{10}$ vary from 0.20 to 0.26, so the conventional BBN process is not spoiled because our estimations, in most of the cases mentioned above, fulfill the severe bound reported for early dark energy: $\Omega_x(z \simeq 10^{10}) < 0.21$ [20].

Acknowledgements L.P.C. thanks the University of Buenos Aires under Project No. 20020100100147 and the Consejo Nacional de Investigaciones Científicas y Técnicas (CONICET) under Project PIP 114-200801-00328 for the partial support of this work during their different stages. M.G.R. is partially supported by Postdoctoral Fellowship programme of CONICET.

References

1. Y. Wang, *Dark Energy* (Wiley-VCH, Berlin, 2010). ISBN 978-3-527-40941-9
2. P. Ruiz-Lapuente (ed.), *Dark Energy: Observational and Theoretical Approaches* (Cambridge University Press, Cambridge, 2010)
3. D. Clowe et al., *Astrophys. J. Lett.* **648**, L109 (2006)
4. M. Bradac et al., *Astrophys. J.* **687**, 959 (2008)
5. R.W. Schnee, [arXiv:1101.5205](#)
6. A.G. Riess et al., *Astron. J.* **116**, 1009 (1998)
7. S. Perlmutter et al., *Astrophys. J.* **517**, 565 (1999)
8. A.G. Riess et al., *Astrophys. J.* **607**, 665 (2004)
9. D.N. Spergel et al., *Astrophys. J. Suppl. Ser.* **170**, 377 (2007)
10. M. Tegmark et al., *Phys. Rev. D* **69**, 103501 (2004)
11. E. Jullo, P. Natarajan, J.P. Kneib, A. d'Aloisio, M. Limousin, J. Richard, C. Schimd, *Science* **329**(5994), 924–927 (2010). [arXiv:1008.4802](#)
12. L.P. Chimento, *Phys. Rev. D* **81**, 043525 (2010)
13. L.P. Chimento, M.G. Richarte, *Phys. Rev. D* **84**, 123507 (2011)
14. L.P. Chimento, M.G. Richarte, *Phys. Rev. D* **85**, 127301 (2012)
15. L.P. Chimento, M.G. Richarte, *Phys. Rev. D* **86**, 103501 (2012)
16. N. Arkani-Hamed, L.J. Hall, C. Kolda, H. Murayama, *Phys. Rev. Lett.* **85**, 4434–4437 (2000)
17. M. Moresco, L. Verde, L. Pozzetti, R. Jimenez, A. Cimatti, *J. Cosmol. Astropart. Phys.* **1207**, 053 (2012)
18. R. Amanullah et al., *Astrophys. J.* **716**, 712 (2010)
19. E. Calabrese, D. Huterer, E.V. Linder, A. Melchiorri, L. Pagano, *Phys. Rev. D* **83**, 123504 (2011)
20. R.H. Cyburt, B.D. Fields, K.A. Olive, E. Skillman, *Astropart. Phys.* **23**, 313 (2005)
21. J. Simon, L. Verde, R. Jimenez, *Phys. Rev. D* **71**, 123001 (2005). [astro-ph/0412269](#)
22. L. Samushia, B. Ratra, *Astrophys. J.* **650**, L5 (2006)
23. D. Stern et al., [arXiv:0907.3149](#)
24. W.H. Press et al., *Numerical Recipes in C* (Cambridge University Press, Cambridge, 1997)
25. A.G. Riess et al., *Astrophys. J.* **699**, 539 (2009). [arXiv:0905.0695](#)
26. E. Komatsu et al., [arXiv:1001.4538](#) [astro-ph.CO]
27. D.S. Sivia, J. Skilling, *Data Analysis: a Bayesian Tutorial* (Oxford University Press, London, 2006)
28. J. Lu, L. Xu, M. Liu, *Phys. Lett. B* **699**, 246 (2011)
29. M.I. Forte, M.G. Richarte, [arXiv:1206.1073](#)
30. L.P. Chimento, M.I. Forte, M.G. Richarte, [arXiv:1206.0179](#)
31. L.P. Chimento, M. Forte, M.G. Richarte, [arXiv:1106.0781](#)
32. L.P. Chimento, M.G. Richarte, [arXiv:1207.1121](#)
33. J.A.S. Lima, J.F. Jesus, R.C. Santos, M.S.S. Gill, [arXiv:1205.4688](#)
34. G. Kremer, *Gen. Relativ. Gravit.* **39**, 965–972 (2007)

Copyright of European Physical Journal C -- Particles & Fields is the property of Springer Science & Business Media B.V. and its content may not be copied or emailed to multiple sites or posted to a listserv without the copyright holder's express written permission. However, users may print, download, or email articles for individual use.